*Kuwait J. Sci.* **47 (1)** pp. 42-49, 2020

# Fabrication of ZnO sensor to measure pressure, humidity and sense vapors at room temperature using the rapid breakdown anodization method

Reem S. Khaleel, Mustafa Sh. Hashim*

*Dept. of Physics, Education College, Mustansiriyah University*

*P.O. Box: 14022 Mustansiriyah University, Baghdad, Iraq*

*Corresponding author: mustmust@uomustansiriyah.edu.iq*

## Abstract

A rapid breakdown anodization process was used to fabricate a ZnO sensor for sensing pressure, humidity and vapors. The X-ray diffraction technique confirmed that this electrochemical process transformed Zn metal to its oxide ZnO. Scanning electron microscope images showed that semispherical ZnO nanoparticles were formed with sizes ranging from 10 to 20 nm. These nanoparticles were deposited on Zn substrates using an electrophoretic deposition method. After deposition, ZnO nanoparticles aggregated and formed large continuous bodies. Atomic force microscopy images showed the vertical growth of ZnO nanoparticles and confirmed the existence of porosity among these particles. Sensing parameters of ZnO to pressure were 0.3417 MΩ/bar for average sensitivity and 1.01 MΩ.bar for hysteresis area. Resistance of ZnO varied exponentially with relative humidity (RH%), and its average humidity sensitivities were 52% (from 20 to 50 RH%) and 95% (from 50 to 90 RH%). The sensing responses to ammonia, ethanol and methanol vapors were recorded using three concentrations (5,10,20 ppm). The sensitivity of the ZnO sensor was greater for methanol, while selectivity was better for ammonia.

**Keywords**: Gas sensor; humidity; nanoparticles; pressure; rapid breakdown anodization; ZnO.

## 1. Introduction

Many studies have been carried out to investigate the physical properties of ZnO and how it can be used for different applications (Rakhshani *et al.*, 2014; Biswas, 2019). Zhu *et al.* (2017) reviewed a gas sensing of ZnO-based gas sensor Ismail *et al.* (2015) reviewed ZnO humidity sensors. Chang *et al.* (2000) and Chou *et al.* (2016) sought to fabricate ZnO humidity and pressure sensors at room temperature. Chae *et al.* (2010) and Samadipakchin *et al.* (2017), among others, studied the production of ZnO nanotubes or nanoparticles using different methods.

Van der Heever *et al.* (2010) investigated the measurement of pressure with fabricated ZnO nanowires by vapor liquid solid method. Vishniakou *et al.* (2016) developed RF sputtered ZnO thin film transistors that exhibit high-performance pressure sensing. None of the previous studies, however, used the Rapid Breakdown Anodization (RBA) technique for the fabrication of ZnO devices. To the best of our knowledge, no researchers have produced such nanoparticles using this simple and inexpensive technique. This research study had three goals. First was to produce ZnO nanotubes or nanoparticles by RBA technique. The second goal was the fabrication of a ZnO sensor for multipurpose use. Third, we investigated whether the RBA process could produce ZnO nanotubes like that of $TiO_2$ under the same RBA conditions.

## 2. Methodology

### 2.1 Preparation of ZnO powder

We utilized the procedure of synthesizing ZnO powder by RBA technique carried out by Park *et al.* (2010). Those researchers prepared titania nanotube powder using this technique. Zn foil was first cleaned with alcohol. The Zn foil had the dimensions 0.1 x 1 x 2 cm. During the anodization process, two Zn foil pieces were immersed in (0.1 M) $HCO_4$ electrolyte. One piece of the foil functioned as an electrode, while the other worked as a counter. Twenty volts was applied between the electrodes, which had a distance of 0.5 cm between them. The anodic process lasted one hour. During this time, the Zn foil sample was completely transformed to a white ZnO powder.

### 2.2 Deposition of produced powders

The electrophoretic deposition (EPD) technique was used to deposit ZnO on the Zn plates. One gram of the produced powders were added to 5 ml of artificial ethanol. The solution was then stirred for 30 minutes. The suspended particles were deposited on the surface of the working electrode after applying 100 volts between the two electrodes for one minute. The deposited samples were dried on a hot plate for 30 minutes. The deposited ZnO was annealed at 600º C for two hours.

### 2.3 Surface and structural characterization of produced layers

The produced ZnO layers were examined by the X-ray diffraction (XRD) technique. The scanning electron microscope (SEM) technique was used to evaluate appearance and particle sizes. Atomic force microscopy (AFM) was utilized to investigate the topographies of the produced samples.

### 2.4 Humidity control and gas pressure measurements

A 1L glass container was employed to test the responses of the fabricated samples to humidity and pressure. To increase or decrease the humidity inside the container, two salts were used. $K_2SO_4$ increased relative humidity (RH%) from 10% to 100%. KOH reduced it to 10%. A hygrometer (KT-908) was used to measure the RH%. Gas pressure was measured inside the container with a pressure gauge (WIKAI). The pressure inside the container was increased by using a simple air motor. To decrease the internal pressure, the valves that control the input and output of gases in the container were adjusted appropriately.

### 2.5 Vapor sensor system

This system consisted of a 6L stainless steel sealed chamber, a controlled vacuum system (to evacuate the gases from chamber after the test), and an ohmmeter to measure sample resistances. Vapor was allowed inside the chamber by using an appropriate chemical solution that was evaporated inside the output unit. Thereafter, the produced vapor was transferred to the partially evacuated chamber. In order to evaporate the small chemical solution and produce the appropriate vapor amount, a micropipette (DRAGONMED) was used. Ammonia was produced by evaporating an ammonia solution (Scharlau-Spain, 32% concentration) according to the following equation (Moore *et al.,* 2004):

$$NH_4OH_{(aq)} \rightarrow NH_{3(gas)} + H_2O_{(l)} . \quad (1)$$

Ethanol and methanol liquids were used to produce their vapors.

## 3. Results and discussion

### 3.1 Characterization of materials

Figure 1 shows the XRD patterns of ZnO before and after annealing. The RBA produced a ZnO powder with a polycrystalline structure. The diffraction peaks of the Zn element (Figure 1) belong to a Zn substrate. After annealing, all peak intensities increased. The crystallinity of ZnO powder also increased.

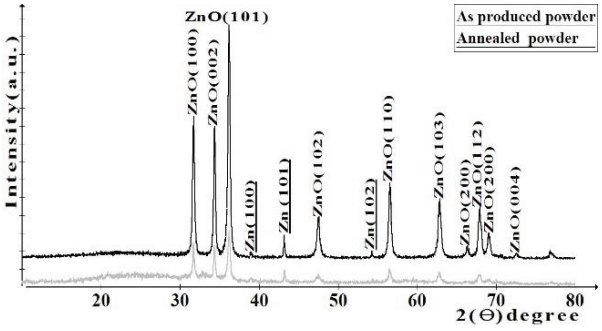


**Fig. 1.** XRD pattern of ZnO powder before and after heat treatment.

Figure 2 shows the AFM image and granularity accumulation distribution on the surface of ZnO. The AFM data for ZnO were an average roughness of 2.71 nm, and the grain size was 61.85 nm. The AFM image (Fig. 2a) shows the vertical growth of nano ZnO particles. This image also confirms the existence of porosity among these particles.

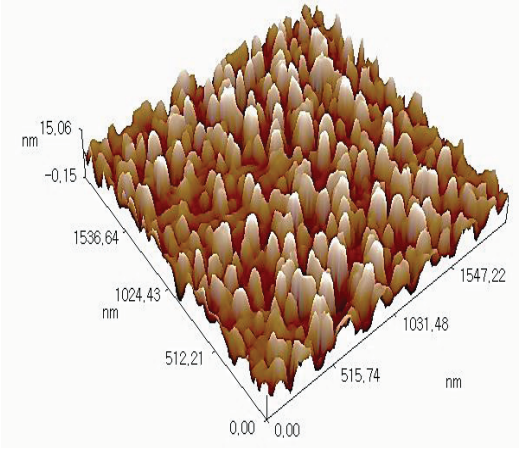


(a)

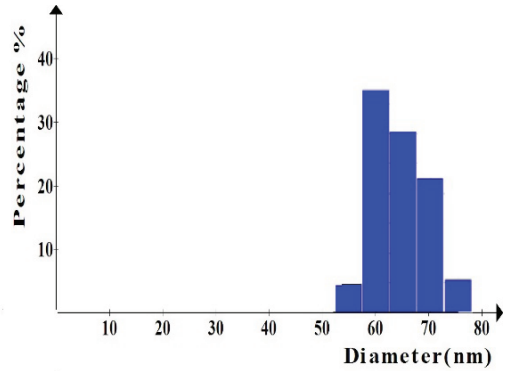


(b)

**Fig. 2.** (a) AFM image (b) granularity accumulation distribution of as deposited ZnO.

Figure 3 shows the SEM images for the deposited ZnO. The particles sizes ranged from 10 to 20 nm. After deposition by the EPD process, the ZnO nanoparticles aggregated and formed large continuous bodies. Figure 3a shows the creation of semispherical nano ZnO particles during RBA. These particles agglomerated and formed into clusters in micro scale (Figure 3b).

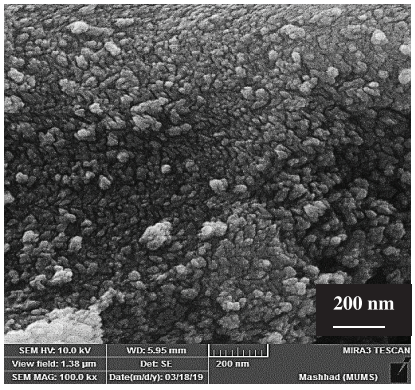


(a)

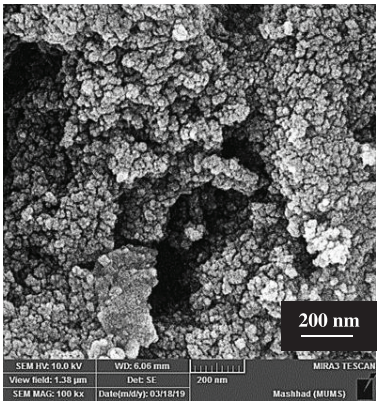


(b)

**Fig. 3.** SEM images of ZnO powder. (a) creation of semispherical nano ZnO particles during RBA (b) nano ZnO particles agglomerated into clusters in micro scale.

There are two reasons behind the agglomeration of these particles. First is the polarity of their surface. A second factor is the exhibition of the piezoelectric effect in the presence of an electric field. Thus, they have an intrinsic anisotropy (Verde *et al.*, 2012).

## 3.2 Sensing characterization

### 3.2.1 Pressure sensing

Figure 4 shows the variation resistance for ZnO ($R_{ZnO}$) as a function of increasing and decreasing pressures. The average sensitivity was 0.3417 MΩ/bar and the hysteresis area was 1.01 MΩ.bar for the sensing parameters of the ZnO pressure sensor. In Figure 4, both curves consist of two regions. The first region, the lowest pressure, is proportionally linear. The second one is a saturation region in which there was high pressure. Thus, the sensor performed better at lower pressures. Wu *et al.* (2003) reported that the resistance of 20 nm ZnO nanocrystals (produced by a micro-emulsion method) rose gradually with increasing pressure, then it decreased.

The dissimilarity between current results shown in Figure 4 and those obtained by Wu *et al*. might be due to different preparation methods for the ZnO nanoparticles (ZNPs).

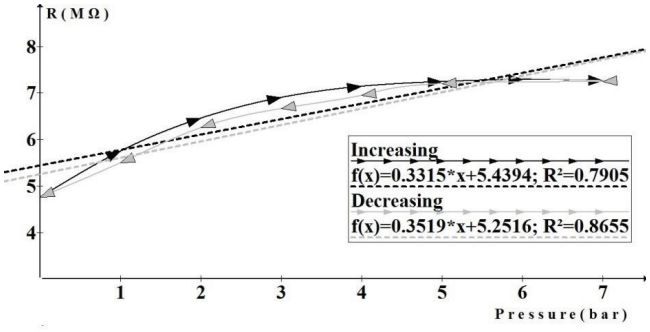


**Fig. 4.** Pressure sensing using prepared ZnO.

### 3.2.2 Humidity sensing

Figure 5 illustrates the variations of resistance as a function of humidity. It shows that $R_{ZnO}$ varies exponentially with humidity. This variation curve fits with the equation $Y=550 *(0.92)^X$. The inset in Figure 5 shows the variation of $R_{ZnO}$ with high levels of RH%. The same behavior is repeated at this scale. (See Pandey *et al.* (2010) for an explanation of the principle of operation for humidity sensing of pure ZnO nanomaterial.)

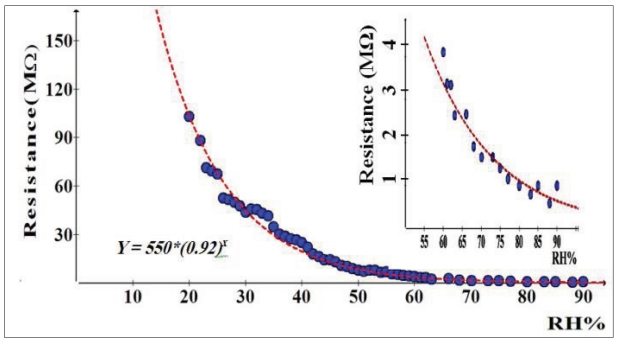


**Fig. 5.** Sensing RH% by ZnO oxide.

On grain surface, $H_2O$ molecules were adsorbed and then reacted with the lattice Zn as:

$$H_2O + O_o + Zn \leftrightarrow 2OH^- + Zn + V_o + 2e^- , \quad (2)$$

where $O_o$ represents the lattice oxygen, and $V_o$ is the vacancy created at the oxygen site (Pandey *et al.* 2010). Because of this reaction, the electrons are collected at the ZnO surface and then the resistance of the ZnO decreases when the RH% increases. Figure 6 shows the percentage of sensitivity of ZnO sensor versus RH%. The average sensitivity, in the range (20 to 50 RH%) was 52% and it increased to 95% in the range (50 to 90 % RH).

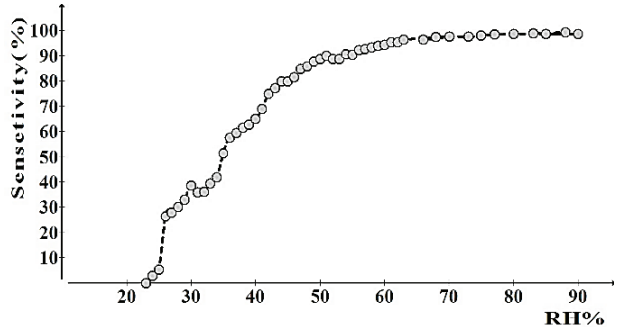


**Fig. 6.** Percentage of sensitivity as a function of RH%.

### 3.2.3 Gas sensing

Figure 7 shows the variation of $R_{gas}/R_{air}$ with time at different concentrations of ammonia.

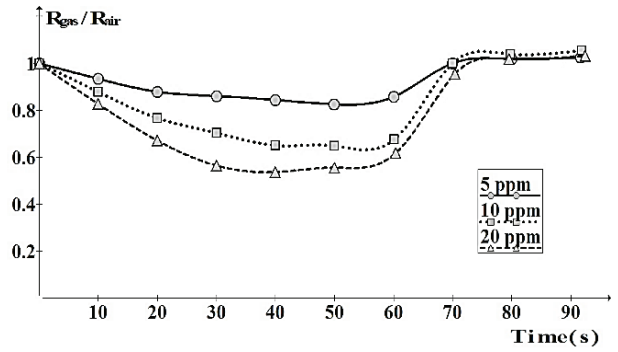


**Fig. 7.** Variation of $R_{gas}/R_{air}$ with time as a function of variable ammonia concentrations.

Response and recovery times were calculated and listed in Table 1. The response increased but the recovery time decreased when ammonia concentrations were increased.

**Table 1.** Variations of response and recovery times with ammonia concentrations.

| Ammonia concentrations | Response time (s) | Recovery time (s) |
|---|---|---|
| 25 | 1.8 | 4.4 |
| 50 | 8.1 | 6 |
| 100 | 11.2 | 7 |

Ul Haq *et al.* (2012) proposed a pathway for the interaction of ammonia with a ZnO surface as:

$$NH_{3(ads)} + 1/2\ O_{2(gas)} + e^- \rightarrow [NH_2.H\text{----}O]^-_{(ads)} \quad (3)$$

$$2\ [NH_2.H\text{----}O]^-_{(ads)} + O^-_{(ads)} \rightarrow N_{2(g)} + 3H_2O + 3e^- , \quad (4)$$

After co-adsorption of ammonia and oxygen on the surface of the sensor, the molecular oxygen captures the electrons of the conduction band and forms $O^-_{(ads)}$. The $[NH_2.H\text{----}O]^-_{(ads)}$ complex forms after the interaction of the two adjacent adsorbed species. Then this complex reacts with the available $O^-_{(ads)}$ and produces free electrons resulting in decreasing sensor resistance (Figure 7).

An $R_{gas}/R_{air}$ decrease over time after ammonia exposure was also observed by Nancy *et al.* (2018). These researchers prepared ZnO nanowires by a thermal evaporation method. The response time and recovery time for their ZnO nanowires were 66 s and 38 s, respectively. Figure 8 shows the behavior of ZnO $R_{gas}/R_{air}$ with time as a function of different ethanol concentrations. Response and recovery times were calculated and listed in Table 2.

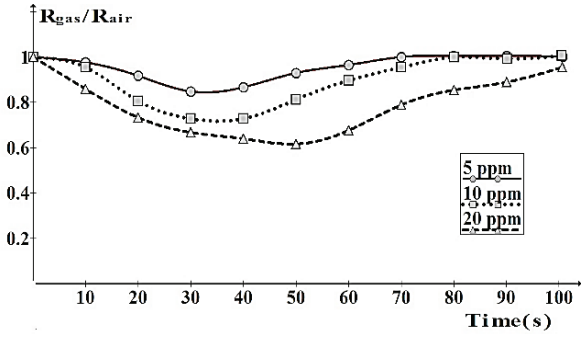


**Fig. 8.** Variation of $R_{gas}/R_{air}$ with time as a function of different ethanol concentrations.

**Table 2.** Variations of response and recovery times with ethanol concentrations.

| Ethanol concentrations | Response time (s) | Recovery time (s) |
|---|---|---|
| 25 | 15 | 20 |
| 50 | 16.8 | 25 |
| 100 | 17.9 | 30 |

Electrons are released back to the surface of the sensor after the reaction of ethanol with the ZnO sensor. This is due to the substitution of the surface-bound oxygen by gas. The reaction with oxygen increases when more ethanol is injected. Finally, ZnO resistance decrease (Hashim *et al.* 2017). In Figure 8, the graph shows an $R_{gas}/R_{air}$ decrease similar to results obtained by Liewhiran *et al.* (2007). In their studies, the ZNPs were prepared by a flame spray pyrolysis technique. The results showed that film cracking, thickness and ethanol concentration have major influence on sensing properties. Table 2 shows that response and recovery times both increased with ethanol concentrations.

The sensor response to methanol is depicted in Figure 9. Gao *et al.* (2013) explained how ZnO resistance decreases after exposure to methanol. The oxygen molecules are chemisorbed on the surface of ZnO when exposed to air. This reaction generates active oxygen species like $O^-$. Subsequently, a surface depletion region forms. Due to the reaction between the ionic oxygen species and methanol, its molecules are oxidized and form an aldehyde or formic acid. Then the electrons are released during this reaction, which results ZnO resistance reduction.

Chandra *et al.* (2012) reported on decreasing $R_{gas}/R_a$ with time as a function of methanol concentrations. They observed that the sensor performed more accurately to methanol vapor when the temperature increased.

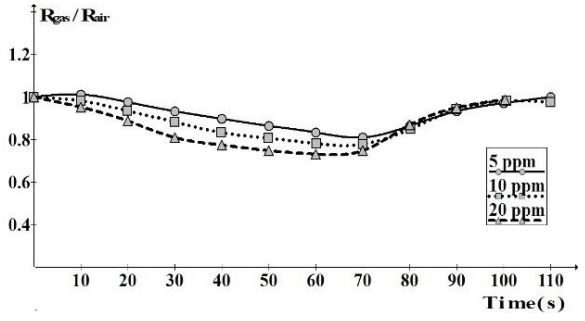


**Fig. 9.** Variation of $R_{gas}/R_{air}$ with time as a function of different methanol concentrations. Both response and recovery times to methanol were calculated (Table 3).

Time increased when methanol concentrations increased. When the sensing mechanism is not based on a simple adsorption-desorption phenomenon at a molecular level, the recovery time could be relatively longer (Ul Haq *et al.,* 2012).

**Table 3.** Variations of response and recovery times with methanol concentrations.

| Methanol concentrations | Response time (s) | Recovery time (s) |
|---|---|---|
| 25 | 16.7 | 25 |
| 50 | 16 | 30 |
| 100 | 13.3 | 33 |

Figure 10 shows the percentage of sensitivity of the ZnO sensor in regards to the tested vapors. Sensitivity increased with a vapor's concentration. Increasing the percentage of sensitivity for methanol and ethanol has a linear behavior, but ammonia has an exponential increase.

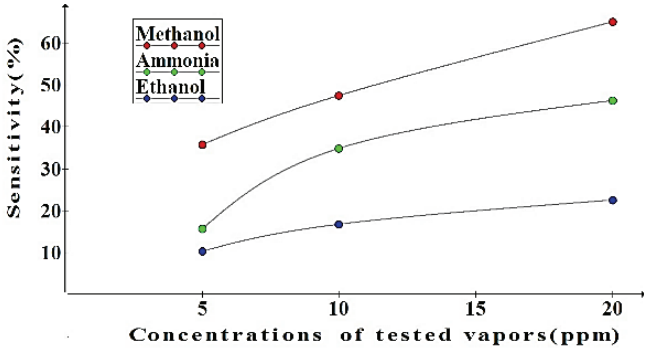


**Fig. 10.** Sensitivity of ZnO sensor to ammonia, methanol and ethanol vapors.

Figure 11 illustrates the calculated selectivity of the ZnO sensor against tested vapors. The largest value was for ammonia. Selectivity experiments for the nanostructured ZnO were carried out at room temperature by Ponnusamy *et al.* (2014). The research showed an excellent response towards ammonia. Its response was better than for acetone, ethanol and methanol. The results of this research agree with this previous study.

Noteworthy is that the RBA technique did not produce ZnO nanotubes under our experimental conditions. Future research into ZnO nanotube production should include different variables.

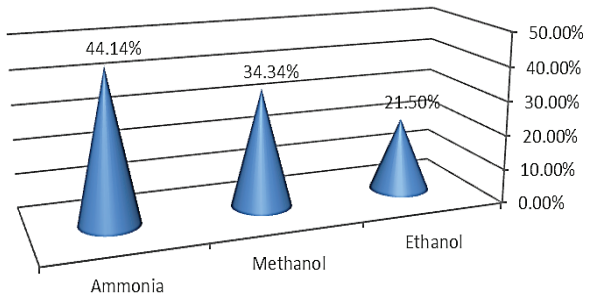


**Fig. 11.** Selectivity of ZnO sensor.

## 4. Conclusions

The RBA method is a good technique for producing active ZNPs that are able to measure pressure, humidity and sense different vapors. The sensitivity of the ZNPs sensor was better for methanol, while selectivity was greater for ammonia. To produce ZnO nanotubes by RBA technique further work with new and different conditions must be applied.

## ACKNOWLEDGEMENTS

We thank the administration of Mustansiriyah University for their support.

## References

**Anasthasiyaa, A.N.A., Kamparaa, R.K., Rai, P.K & Jeyaprakash, B.G. (2018).** Gold functionalized ZnO nanowires as a fast response/recovery ammonia sensor, Applied Surface Science, **449**(15): 244-249.

**Antony, R.P., Mathews, T., Dasgupta, A., Dash, S., Tyagi, A.K., *et al.* (2011).** Rapid breakdown anodization technique for the synthesis of high aspect ratio and high surface area anatase $TiO_2$ nanotube powders. Journal of Solid-State Chemistry, **184**: 624–632.

**Biswas, S. (2019).** Investigation of the insulator to half-metal transition in Cr-doped ZnO at low temperature (19K) wurtzite structure. Kuwait Journal of Science, **46**(2): 44-51.

**Chang, C.C. & Fang, S.K. (2000).** A study of the design of ZnO thin film pressure sensors. International Journal of Electronics, **87**(8): 1013-1023.

**Chae, K.W., Zhang, Q., Kim, J.S., Jeong, Y.H. & Cao, G. (2010).** Low-temperature solution growth of ZnO nanotube arrays. Beilstein Journal of Nanotechnology, **1**: 128–134.

**Chandra, S., Pandya, H.J. & Vyas, A.L. (2012).** A methanol sensor incorporating nanostructured ZnO and integrated microheater on thermally isolated planar MEMS platform. Sensor Devices. The Third International Conference on Sensor Device Technologies and Applications. Rome, Italy, 20-25 August, pp. 83-88.

**Chou, K.S., Lee, C.H. & Liu, B.T. (2016).** Effect of microstructure of ZnO nanorod film on humidity sensing. Journal of the American Ceramic Society, **99**(2): 531-535.

**Gao, Q., Zheng, W., Wei, C.D. & Lin, H.M. (2013).** Methanol-sensing property improvement of mesostructured zinc oxide prepared by the nanocasting strategy. Journal of Nanomaterials, **2013**(3): 1-7.

**Hashim, M.S., Khaleel, R.S., (2017).** Al-Bahir Quarterly Adjudicated Journal for Natural and Engineering Research and Studies, **5**(9): 45-51.

**Ismail, A.S., Mamat, M.H. & Rusop, M. (2015).** Humidity sensor-A review of nanostructured zinc oxide ZnO-based humidity sensor. Advanced Materials Research, **1109**: 395-400.

**Liewhiran, C. & Phanichphant, S. (2007).** Influence of thickness on ethanol sensing characteristics of doctor-bladed thick film from flame-made ZnO Nanoparticles. Sensors (Basel), **7**(2): 185-201.

**Moore, J.T. (Ed.) (2004).** Chemistry made simple. New York, Three Rivers Press. pp.190.

**Panaitescu, E., Richter, C., & Menon, L. (2008).** A study of titania nanotube synthesis in chloride-ion-containing media. Journal of the Electrochemical Society, **155**(1) E7-E13.

**Pandey, N.K., Karunesh, T. (2010).** Morphological and relative humidity sensing properties of pure ZnO nanomaterial. Sensors & Transducers Journal, **122**(11): 9-19.

**Park, S.J., Paek, Y.K., Lee, H. & Kim, Y. (2010).** Lithium ion insertion in titania nanotube powders synthesized by rapid breakdown anodization. Electrochemical and Solid-State Letters, **13**(7): A85-A87.

**Ponnusamy, D. & Madanagurusamy, S. (2014).** Nanostructured ZnO films for room temperature ammonia sensing. Journal of Electronic Materials, **43**(9): 3211–3216.

**Rakhshani, A.E., Bumajdad, A., Kokaj J. & Thomas S. (2014).** Preparation and characterization of nitrogen doped ZnO films and homojunction diodes. Kuwait

Journal of Science, **41**(1): 107-127.

**Samadipakchin, P., Mortaheb, H.R. & Zolfaghari, A. (2017).** ZnO nanotubes: Preparation and photocatalytic performance evaluation. Journal of Photochemistry and Photobiology A: Chemistry, **337**: 91-99.

**Ul Haq, I. & Azad, A.M. (2012).** Experimental artifacts for morphological tweaking of chemical sensor materials: Studies on ZnO. Sensors (Basel), **12(**6): 8259-8277.

**Van der Heever, T.S. (2010).** A zinc oxide nanowire pressure sensor, Master's thesis, University of Stellenbosch, South Africa.

**Verde, M., Peiteado, M. Caballero. A.C., Villegas, M. & Ferrari, B. (2012).** Electrophoretic deposition of transparent ZnO thin films from highly stabilized colloidal suspensions. Journal of Colloid Interface Science. **373**(1): 27-33.

**Vishniakou, S. (2016).** Zinc oxide thin film transistor pressure sensors, Ph.D.thesis, University of California, San Diego.

**Wu, Z.Y., Bao, Z.X., Zou, X.P., Tang, D.S., Liu, C.X. *et al.* (2003).** Conductance and phase transition of free standing ZnO nanocrystals under high pressure. Materials Science and Technology. **19**:981-984.

**Zhu, L. & Zeng, W. (2017).** Room-temperature gas sensing of ZnO-based gas sensor: A review. Sensors and Actuators A: Physical, **267**: 242-261.

**Submitted :** 09/05/2019

**Revised :** 24/07/2019

**Accepted :** 30/07/2019

# صناعة مستشعر أكسيد الزنك لقياس الضغط والرطوبة والأبخرة في درجة حرارة الغرفة بواسطة تقنية الأَنودة السريعة

**ريم صالح خليل، مصطفى هاشم**
قسم الفيزياء، كلية التربية، الجامعة المستنصرية
الجامعة المستنصرية، بغداد، العراق

## الملخص

تم استخدام عملية الأنودة السريعة لتصنيع مستشعر أكسيد الزنك لاستشعار الضغط والرطوبة والأبخرة. حولت هذه العملية الكهروكيميائية معدن الزنك إلى أكسيد الزنك بواسطة تقنية حيود الأشعة السينية. تشكلت جسيمات متناهية الصغر من أكسيد الزنك نصف كروية بأحجام تراوحت من 10 إلى 20 نانومتر، كما أظهرت صور المسح بواسطة المجهر الإلكتروني. تم ترسيب هذه الجسيمات النانوية على ركائز الزنك باستخدام طريقة الترسيب الكهربي. بعد عملية الترسيب، تجمعت جسيمات أكسيد الزنك النانوية وتشكلت على هيئة أجسام كبيرة مستمرة. أظهرت الصور المأخوذة عن طريق مجهر القوة الذرية النمو العمودي لجسيمات أكسيد الزنك النانوية وأكدت على وجود مسامات بين هذه الجسيمات. وكانت معايير استشعار أكسيد الزنك للضغط (0.3417 ميجا أوم / بار) لمتوسط الحساسية و(1.01 ميجا أوم / بار) لمنطقة التباطؤ المغناطيسي. تباينت مقاومة أكسيد الزنك بشكل تصاعدي مع الرطوبة النسبية(RH%) وكان متوسط الحساسية للرطوبة 52 % (في حدود 20 إلى 50) و 95 % (في حدود 50 إلى 90). تم تسجيل استجابة لاستشعار أبخرة الأمونيا والإيثانول والميثانول بتركيزات مختلفة. كانت حساسية مستشعر أكسيد الزنك أكبر للميثانول بينما كانت الانتقائية أفضل للأمونيا.